Escrivá Cerdán, C.; Blasco Tamarit, ME.; García García, DM.; García Antón, J.; Akid, R.; Walton, J. (2013). Effect of temperature on passive film formation of UNS N08031 Cr-Ni alloy in phosphoric acid contaminated with different aggressive anions. Electrochimica Acta. 111:552-561. doi:10.1016/j.electacta.2013.08.040.

Effect of temperature on passive film formation of UNS N08031 Cr-Ni alloy in phosphoric acid contaminated with different aggressive anions

Escrivà-Cerdán, C.[a], Blasco-Tamarit, E.[a], García-García, D.M.[a], García-Antón, J.[a,*], Akid, R[b], Walton, J[b]

[a]*Ingeniería Electroquímica y Corrosión (IEC). Departamento de Ingeniería Química y Nuclear. ETSI Industriales. Universitat Politècnica de Valencia. Camino de Vera s/n, 46022 Valencia, Spain.*

**Tel. 34-96-387 76 39, Fax. 34-96-387 76 39, e-mail. jgarciaa@iqn.upv.es*

[b]*Corrosion & Protection Centre. School of Materials. University of Manchester. Manchester M13 9PL, UK.*

ABSTRACT

The influence of temperature and the effect of aggressive anions on the electrochemical behaviour of UNS N08031 stainless steel in a contaminated phosphoric acid solution were evaluated. Stabilisation of the passive film was studied by potentiodynamic polarisation curves, potentiostatic tests, Electrochemical Impedance Spectroscopy (EIS) measurements, Mott-Schottky analysis and X-ray Photoelectron Spectroscopy (XPS). The stability of the passive film was found to decrease as temperature increases. The film formed on the stainless steel surface was a n-type semiconductor and the XPS spectrum revealed the presence of fluoride ions.

Keywords: Stainless steel, Acid solution, EIS, Mott-Schottky, XPS

1. INTRODUCTION

Stainless steels have excellent corrosion resistance, resulting from a thin and protective passive film, which prevents the metal from reacting with corrosive environments. However, the action of some aggressive anions on passive metals can lead to a locally or generally increased dissolution rate [1]. More specifically, in the phosphoric acid production industry, corrosion problems are mainly caused by the presence of impurities such as fluoride (F^-) or chloride (Cl^-) ions [2], which act as aggressive ions increasing the risk of corrosion damage of processing equipment depending on the type of stainless steel used. In this respect, the use of highly alloyed materials in aggressive environments is common practice in industrial applications [3].

In order to prevent corrosion, it is important for stainless steels to maintain a stable passive film with, in the event of damage to the film, a rapid passivation rate even in severe corrosive environments [4]. Thus, it is important to quantify the kinetics of passive film formation on stainless steels.

The behaviour of stainless steels in aqueous acid solutions has been widely investigated with numerous studies reporting on the passivity and corrosion behaviour of austenitic stainless steels in sulphuric acid solutions [5-9] and phosphoric acid solutions [10-13]. Other studies [3, 14, 15] have been published on the electrochemical behaviour of stainless steels in mixtures of chloride and fluoride aqueous solutions. However, only very limited information appears available on the corrosion and passive behaviour of super-austenitic stainless steels in phosphoric acid solution, specifically solutions polluted with various aggressive ions.

The aim of this research was to investigate the corrosion behaviour of a highly alloyed austenitic stainless steel (UNS N08031) in phosphoric acid polluted with sulphate, chloride and fluoride ions, simulating typical industrial conditions [16]. The effects of the solution temperature on the electrochemical behaviour and the passivation kinetics were evaluated. Semiconducting properties were also investigated and XPS analysis allowed the study of the chemical composition on the surface of the stainless steel.

2. EXPERIMENTAL

2.1. Material and test solution

The material tested was a highly alloyed austenitic stainless steel UNS N08031 (Alloy 31) provided by Thyssen Krupp VDM. The material composition of this alloy is shown in **Table 1**. Alloy 31 electrodes were cylindrically shaped (8 mm in diameter and 55 mm long). The working surface of the specimens exposed to the test solution was 0.5 cm^2 and all other areas of the electrode were covered with a polytetrafluoroethylene (PTFE) coating.

Prior to immersion, electrodes were abraded with wet emery paper of decreasing grit size (500 - 4000), followed by rinsing with distilled water and dried within a stream of air.

Samples were tested in a polluted 40 wt.% phosphoric acid solution with 2 wt% of H_2SO_4, 0.06 wt.% KCl and 0.6 wt.% HF, typical concentrations for the phosphoric acid industry [16].

2.2. Electrochemical measurements

The electrochemical tests were performed in a PTFE vertical three-electrode cell held at a constant temperature, which consisted of a platinum (Pt) counter electrode, a silver/silver chloride (Ag/AgCl)/3 M potassium chloride (KCl) reference electrode and the specimen as the working electrode. The solution was deaerated by purging with N_2 for 20 min before the test. A nitrogen atmosphere was maintained over the liquid surface during the duration of the test. The experiments were conducted under controlled temperature conditions at 20, 40, 60 and 80 ºC in order to study the influence of temperature on the corrosion behaviour of Alloy 31.

2.2.1. Open Circuit Potential measurements

The open circuit potential was measured for 1 hour in the test solution. The average value of the potentials recorded during the last 300 seconds was recorded as the value of the OCP according to ASTM G-5 [17].

2.2.2. Potentiodynamic tests

Potentiodynamic polarisation curves were determined by using a Solartron 1278 potentiostat. Before each polarisation measurement, the working electrodes were

initially polarised in four steps from the OCP values to 0 $V_{Ag/AgCl}$. This potential was maintained for 1 hour in order to remove the air-formed oxide on the surface [18-20] and to create reproducible initial conditions. The sample was then polarised anodically at a scan rate of 0.1667 mV/s from 0 $V_{Ag/AgCl}$ in the anodic direction, according to ASTM G5 [17], the potential scan was reversed when the current density reached 10 mA/cm^2.

The polarisation curves were used to obtain information about general electrochemical behaviour and to determine the following electrochemical parameters; corrosion current density *(i_{corr})*, corrosion potential *(E_{corr})* and transpassive potential *(E_{tr})*, defined as the potential at which the current density reaches the value of 100 $\mu A/cm^2$. The current density before E_{tr} is almost constant during a range of potentials where the passive current density *(i_{pas})* can be estimated as an average of this range.

2.2.3. Potentiostatic tests

Potentiostatic passivation tests were performed using an Autolab PGSTAT302N potentiostat in order to obtain the current transient at a constant applied potential. The imposed potential 0.8 $V_{Ag/AgCl}$ was selected according to the potentiodynamic curves, since this potential lies within the passive range. Prior to each measurement, the working electrodes were polarised to 0 $V_{Ag/AgCl}$ for 1 hour to remove the passive film formed in air [18-20]. The chosen potential (0.8 $V_{Ag/AgCl}$) was then applied for 1 hour and the potentiostatic current density transients were recorded.

2.2.4. Impedance and capacitance tests

Once the passive film was formed and just after the potentiostatic tests, the electrochemical impedance spectroscopy (EIS) and capacitance measurements were performed. EIS tests were taken at the chosen potential (0.8 $V_{Ag/AgCl}$) in the range between 10^5 and 10^{-3} Hz with voltage amplitude ±5 mV. Fitting was performed with Z-view software. Capacitance measurements were also taken on the anodic films formed at 0.8 $V_{Ag/AgCl}$, at a frequency of 3 kHz using a 10 mV rms ac signal and a step rate of 25 mV, in the cathodic direction.

2.2.5. XPS analysis

The chemical composition of the surface films formed on Alloy 31 were investigated using a *Kratos Axis Ultra* X-ray photoelectron spectrometer (Kratos Analytical Ltd, Manchester, UK) with a monochromatic Al Kα radiation source of 12 keV, 10 mA. Wide scans were acquired at 80 eV pass energy from 1100 eV to 0 eV binding energy, and high-energy resolution scans were acquired through photoelectron regions of interest at 20 eV pass energy. Sample charging was minimised using a flood of low energy electrons from a linear filament operated with 0.18 A current, 3 V bias and 2.9 V charge balance, and charge correction made by reference to the hydrocarbon peak at 285.0 eV binding energy. The area analysed was 700 μm x 300 μm. The data was quantified by measuring photoelectron peak areas, using theoretical relative sensitivity factors following correction for the intensity/energy response of the instrument [21]. All data processing was carried out using CasaXPS (Casa Software Ltd, Teignmouth, UK).

3. RESULTS AND DISCUSSION

3.1. Open Circuit Potential

Figure 1 presents the open circuit potential measurements for Alloy 31 in the solution studied at 20, 40, 60 and 80 ºC. At all temperatures the potential shifted towards more positive values immediately after immersion in solution. The ennoblement of the potential observed in **Figure 1** is attributable to changes in the pre-immersion air-formed oxide film and further thickening of the oxide film as a result of the interaction between the electrolyte and the metal surface [22]. The growth of the oxide film continues until the film acquires a thickness that is stable in the electrolyte. Alloy 31 contains 26.75% chromium, which is responsible for the passive properties of the alloy. Thus, during the OCP test the Cr_2O_3-containing passive film grew on the electrode surface, shifting the OCP value to higher potentials [23].

The OCP values of Alloy 31 in the phosphoric acid solution are summarised in **Table 2**. It can be seen that OCP values shift towards more positive values as temperature increases, which is justified by the passive nature of Alloy 31. It is well known that temperature increases the kinetics of corrosion reactions [24-28]; however it also promotes rapid growth of passive films on metallic surfaces [29-31], resulting in the ennoblement of the metal.

3.2. Potentiodynamic polarisation behaviour

Potentiodynamic polarisation curves for Alloy 31 in contaminated phosphoric acid solution were obtained at 20, 40, 60 and 80 ºC to evaluate the effect of temperature on the general corrosion resistance of the metal (**Figure 2**).

Alloy 31 displays similar polarisation curves at all temperatures showing a passive range in which the current density remains almost stable. However, as temperature increases above 40 ºC, the current density values in this region exhibit an increasing trend. This fact indicates that the increase of temperature induces a restriction of passivity range of the material [32]. As a consequence, the transpassive potential E_{tr}, at which the breakdown of the passive film occurs, is observed to decrease as temperature increases. Polarisation curves show that Alloy 31 is passive at all temperatures since a passivation range is observed.

Temperature affects the cathodic reaction as observed on the potentiodynamic curves, since the cathodic current densities increased with temperature (**Figure 2**). This shows that increasing temperature favours the cathodic reaction [24, 32, 33] and more specifically, it favours the hydrogen evolution reaction (HER); consequently increasing temperature also favours the kinetics of anodic dissolution of the metal.

The presence of aggressive ions, such as chloride, sulphate and fluoride in solution, accelerates the anodic process; therefore, the harmful effect of temperature is greater in this solution because these ions should make the oxide dissolution easier [10, 34-36].

From the potentiodynamic polarisation curves, corrosion potential (E_{corr}), corrosion current density (i_{corr}), passive current density (i_p) and the transpassive potential (E_{tr}) were obtained and are summarised in **Table 3**. It can be observed that E_{corr} and i_{corr} increase with temperature, as well as i_p also showed an increase with increasing temperature.

The increase of E_{corr} and i_{corr} seems to be related to the enhancement of the cathodic reaction with temperature [24, 37, 38]. The corrosion potentials followed the same tendency as the OCP values, although E_{corr} values are slightly lower, indicating that the OCP values of Alloy 31 in this solution are close to the cathodic-anodic transition. This phenomenon suggests that Alloy 31 under these conditions will be close to the equilibrium potential. This behaviour was also reported for steels in fluoride containing solutions [2]. Although the i_{corr} values are observed to increase with temperature; this parameter abruptly increases from 40 ºC, suggesting an accelerating effect of aggressive ions at elevated temperatures.

The trend of increasing passive current density, i_p with increasing temperature, is explained by the fact that the increase of temperature favours the growth of the passive film [24]. The passive film on Alloy 31 consists of an inner layer, which is mainly composed of Cr_2O_3 [34, 39, 40], since Alloy 31 contains high Cr content. The outer layer of the passive film is probably enriched in iron phosphates. In this context, several studies have reported that phosphate species are incorporated into the outer part of the passive film during the passivation process [41-44]. This statement is confirmed in the XPS analysis (section 3.6), in which the binding energy of the P 2p photoelectron peak at 133.8 eV for all samples indicates that it is present as phosphate.

The transpassive potential E_{tr}, which is defined as the potential at which the current density reaches the value of 100 $\mu A/cm^2$, is observed to decrease as temperature increases. Consequently, Alloy 31 is less corrosion resistant as temperature increases in the phosphoric acid solution polluted with 2% H_2SO_4, 0.06% KCl and 0.6% HF. These results reveal that the passive films formed at lower temperatures are significantly less defective and more resistant to film breakdown than those formed at higher temperatures, as reported by several authors [13, 22, 24, 30, 37, 38, 45].

3.3. Potentiostatic tests

The current-time transients of Alloy 31 obtained at 0.8 $V_{Ag/AgCl}$ in the contaminated phosphoric acid solution at different temperatures are shown in **Figure 3**. The values of current density recorded during the potentiostatic tests give the total current resulting from the film formation and the dissolution of Alloy 31 in the solution studied [46].

In **Figure 3(a)**, it is initially observed that the current density decreases rapidly with time at all temperatures. This is attributed to the nucleation and growth of the passive film at a rate higher than that of metal dissolution. All current-time transients show that further increase in time resulted in a relatively steady state current density *(i_{ss})*, as shown in the enlargement of **Figure 3(a)**, indicating the formation of a passive film on the surface of Alloy 31. This i_{ss} is observed to increase with increasing temperature (**Table 4**), indicating a reduction in the protective nature of the passive film. However, it is noteworthy that at higher temperatures, increasing immersion times resulted in some current density fluctuations. Some authors have associated these fluctuations,

which are clearly observed at 80 ºC, to either nucleation or metastable pitting events [18, 47].

Figure 3(b) presents the *log i-log t* plots for Alloy 31 in the solution studied at different temperatures, in which the anodic current transients have been divided into three stages, as reported by other authors for aluminium and its alloys [48, 49] and for stainless steels [13, 50, 51] and. In all cases, the anodic current of the first stage was constant, indicating that the rate of oxide formation equalled the rate of oxide dissolution so that the oxide film hardly grew. The period at which the current density *(i)* starts to decrease with time can be seen in stage 2 and this belongs to a transition period. In stage 3, the anodic current density decreased linearly with time in the logarithmic scale, which is clearly observed in the transient obtained at 20 ºC. The current density drop was due to the rate of the passivating oxide film dominating over the dissolution rate on the bare surface [48-51]. However, as the temperature increased from 20 ºC to 80 ºC, the log-log plots exhibit an ascending range from the moment just after the induction time (t_m), which some authors have attributed to film breakdown caused by the growth of pits below E_{tr} [4, 48, 49, 51]. From representations in **Figure 3(b)**, it is clearly observed that these induction times decrease with temperature (arrowed in Figure 3b) indicating that temperature affects negatively to the protective properties of passive films formed on Alloy 31.

The time-current density relationship can be expressed by the following empirical equation [18, 46, 48-52]

$$i = A \cdot t^{-n} \tag{1}$$

where *i* denotes the anodic current density consumed in the building of the passive film, *A* is a constant, *t* is the time, and *n* is the passivation index, which is a constant value for a given environment-metal system. This parameter can be obtained from the linear region slope of the log *i* vs log *t* plot (**Figure 3(b)**) and it has been considered as an indirect measure of the rate of formation of the passive film upon the fresh metal surface, being primarily dependent upon the applied anodic potential [4, 18, 48, 50]. According to the literature [53, 54] $n = 1$ indicates the formation of a compact, highly protective passive film, while $n = 0.5$ indicates the presence of a porous film growing as a result of a dissolution and precipitation process.

Based upon equation (1), the passivation rate parameter *n* is determined as a function of temperature after 1 hour of stabilisation of the passive films at 0.8 $V_{Ag/AgCl}$. **Table 4** summarizes the values of *n* for Alloy 31. The slight decrease of this parameter with temperature is an indication that the protective properties of the passive films decrease with increase in temperature and that the passive film grows more slowly as temperature increases.

Figure 4 presents LEICA microscope images of Alloy 31 surfaces observed after the potentiostatic tests at different temperatures. The defects observed on the surfaces are considered to be corrosion pits.

The formation of pit-like defects is more probable as temperature increases, especially in the presence of chloride ions, as has been reported previously [28, 35, 55]. Moreover,

according to other publications [2, 9], the presence of F^- enhances the local corrosion susceptibility of stainless steels.

3.4. Electrochemical impedance analysis

Electrochemical impedance spectroscopy was employed to investigate the relative stability of the passive films formed on Alloy 31 in the contaminated phosphoric acid solution. EIS measurements were recorded under potentiostatic conditions after 1 hour of passive film formation at the applied potential of 0.8 $V_{Ag/AgCl}$ at the different temperatures studied.

The stability of the system is crucial for the validity of EIS measurements and, in this sense the electrochemical system should comply with three requirements formulated for the constraints of the linear system theory (LST), i.e. causality, linearity and stability [56-58]; otherwise the EIS results will be invalid. Validatation of the EIS results is by way of the Kramers-Kronig (K-K) transformation [57]. The K-K transforms have been applied to the experimental impedance data by transforming the real axis into the imaginary axis and the imaginary axis into the real axis and then comparing the transformed quantities with the respective experimental data. As an example, **Figure 5** presents a comparison between experimental data obtained at 20 ºC and the corresponding K-K transforms. Good agreement between the experimental and calculated results confirms the compliance of the system with the linear system theory.

Figure 6 shows the impedance spectra obtained at different solution temperatures, presented in both Bode and Nyquist formats. Two time constants can be distinguished

in the 20 ºC impedance spectra shown in **Figure 6(a)**, while at the higher temperatures the lower frequency time constant is not distinguishable. The modulus phase is always lower than 90º indicating that this behaviour can be interpreted as a deviation from ideal capacitor behaviour. On this basis, a constant phase element (CPE) was applied to account for the non-ideal behaviour of the capacitive elements. Deviation from ideal behaviour was considered to be due to various factors including; surface heterogeneity and roughness, impurities, dislocations, grain boundaries, adsorption of species and the formation of porous layers [59, 60]. The impedance of this element is defined [56] as:

$$Z_{CPE} = \frac{1}{Q \cdot (j\omega)^{\alpha}} \tag{2}$$

where Q is the CPE constant, ω is the angular frequency (rad/s), j^2=-1 is the imaginary number and α is the CPE exponent. Depending on α, CPE can represent resistance ($\alpha = 0,\ Z_0 = R$), capacitance ($\alpha = 1,\ Z_0 = C$) or Warburg impedance ($\alpha = 0.5,\ Z_0 = W$).

At high frequencies (between 10^4 and 10^5 Hz) the absolute impedance curve in the Bode plot, is almost independent of the frequency with a phase angle of 0º, representing the electrolyte resistance *(R_s)*.

From the Nyquist diagrams (**Figure 6(b)**) it is clearly distinguishable that two types of electrochemical equivalent circuits would be necessary in order to model the data. In this sense, the diagram at 20 ºC (**Figure 6(b)**) depicts a somewhat unfinished capacitive arc whereas at higher temperatures the diagrams present a lower frequency inductive-

loop. The latter case may be attributed to the relaxation process obtained by adsorption species such as halide ions F^-_{ads}, Cl^-_{ads} and H^+_{ads}, on the stainless steel surface [61], and the former case has been explained as the response of an inhomogeneous film composed of a compact inner layer and a less compact (porous) outer layer [62-66].

Based on this behaviour, two different equivalent electrical circuits have been constructed, see **Figure 7(a)** relating to the response at 20 ºC. This equivalent circuit has been previously reported [18, 61-69]. The high frequency time constant is represented by the resistance of the solution in the defects of the porous film (R_1) and the double layer capacitance in the defects (C_1). The second time constant at low frequencies is assigned to the areas covered with the passive oxide film (protective oxide) and it is represented by the R_2/C_2 parallel combination. Both parameters, R_2 and C_2, represent the electrical resistance and the capacitance of the passive oxide film formed as an inner layer on Alloy 31 [66].

The theoretical simulated impedance parameters for the Alloy 31 tested under these conditions were computed using Z-view software and the results are summarised in **Table 5**. The quality of data fitting to the equivalent circuits proposed was evaluated with the chi-squared (χ^2) values, which in all cases were lower than 10^{-3}, and the error percentages of the individual components of the equivalent circuits fitted. This fact is also justified by the similarity between the experimental and the theoretical data, both shown in **Figure 6**.

On the other hand, the spectra at 40, 60 and 80 ºC depicted the same high-frequency capacitive loops as the ones commented at 20 ºC. However, a characteristic feature of

the first spectra was the appearance of an inductive loop at low frequencies. This loop has been reported by other researchers [70-73] and it is mainly due to the relaxation of the corrosion product on the electrode surface [70, 74], which has been observed to become more dominant as the temperature increases (**Figure 6(b)**). The equivalent electrical circuit proposed for solution temperatures above 20^{o}C is shown in **Figure 7(b)** and consists of the following elements: C_1 represents the capacity of the metal/film/electrolyte interface, R_1 is the outer porous layer resistance, C_2 and R_2 are the capacitance and the resistance of the inner oxide layer and *RL* element (resistance and inductance) is attributed to the corrosion products' relaxation [70, 74]. A summary of the electrochemical properties derived from the EIS data is is presented in **Table 5**.

The CPE used in the equivalent electric circuits of **Figure 6** has been converted into a pure capacitance (C) by means of the following equation [66, 75]:

$$C = \frac{(Q \cdot R)^{1/\alpha}}{R} \tag{3}$$

According to the electrical parameters shown in **Table 5**, the resistance of the inner oxide layer (R_2) is larger than the value associated with the outer porous layer (R_1), which is consistent with the chosen physical model for the representation of these impedance spectra. In this sense, the results indicate that the protection provided by the passive film was predominantly due to the barrier layer, as reported in other studies [63, 66, 76]. The resistance of the solution, R_s remains almost constant in all tests. In fact, the frequency independence of the absolute impedance curve (Figure 6(a)) with phase angle of 0^{o} represents this feature.

With respect to the parameters associated with the outer porous layer, the values of R_1 suggest that this layer was thinner and porous, as reported previously [63, 66] and C_1 represents the double layer capacitance, the value of which hardly changes with change in temperature [56, 66]. This is in contrast to the trend of the parameters associated with the inner oxide layer R_2 and C_2, which are more affected by temperature. R_2 clearly decreases when temperature increases, indicating that the films' electrical conductivity increases and the barrier layer capacitance C_2, in general, increases considerably with temperature. This behaviour has been previously explained by the fact that the inner oxide film becomes thinner [66] and the abrupt increase from the temperature of 40 ºC clearly indicates that the transpassive region is near to 0.8 $V_{Ag/AgCl}$ [66] and therefore transpassive dissolution of the passive film is happening under these conditions, which is also in accordance with the data presented in **Figure 4**. Finally, the parameters associated with the inductive loop shows that *RL* decreases with increase in temperature (**Table 5**) indicating that absorption of intermediate species through the passive film is more probable at higher temperatures [77].

The EIS results demonstrate that increasing solution temperature negatively affects the protective properties of the passive films formed on Alloy 31. Moreover, as temperature increases, the halide species of the corrosion product layer formed on the specimens' surface are more likely to be transported through to the Alloy 31. As a consequence, the aggressive ions, F^-, Cl^- and SO_4^{2-}, are able to reduce the protective properties of the passive film of Alloy 31, which is consistent with the results obtained from the polarisation and potentiostatic tests, and the images shown in **Figure 4**.

3.5. Mott-Schottky analysis

Passive films formed on most metals and alloys have been demonstrated to exhibit semi-conductive behaviour [78-81], which can be described by Mott-Schottky (M-S) analysis. In order to explore the changes in the electronic properties of the passive film on Alloy 31 in contaminated phosphoric acid solution, M-S analysis was carried out after the specimens had been passivated for 1 h under the same conditions described above. The imaginary part of the impedance *(Z'')* was measured at a frequency of 3 kHz as a function of the potential, as the potential was swept in the negative direction at a sweep rate of 25 mV/s. This high sweep rate was used to avoid electro-reduction of the oxide layer and the change in the film thickness during the measurements [67]. From the measured values of *Z''* in these tests, and the previously determined CPE α exponents, it was possible to calculate the CPE parameter, *Q*, and then the electrode capacitance using expression (3).

Based on Mott-Schottky theory [82], the semiconducting characteristics of passive films can be explored by measuring the capacitance of the interface layer developed in the passive film and the Helmholtz layer, as a function of the applied electrode potential. The measured capacitance can be described by this theory as: $1/C = 1/C_{SC} + 1/C_H$ where C_{SC} and C_H represent the space charge and the Helmholtz capacitance respectively. However, since the capacitance of the space charge layer is very small compared with that of the Helmholtz layer, the measured interfacial capacitance can be regarded as that of the space charge layer when the potential perturbations are applied with a sufficiently high frequency [18]. According to this theory, DeGryse et al. [83] and Gerischer et al. [84] obtained the following relationships between the total

capacitance and the potential difference for passive films on iron and stainless steels. Thus, the space charge capacitance of p- and n-type semiconductors is given by Eq. (4) and (5), respectively:

$$\frac{1}{C^2} = \frac{1}{C_H^2} - \frac{2}{\varepsilon \varepsilon_0 q N_A}\left(E - E_{FB} - \frac{kT}{q}\right) \quad (4)$$

$$\frac{1}{C^2} = \frac{1}{C_H^2} + \frac{2}{\varepsilon \varepsilon_0 q N_D}\left(E - E_{FB} - \frac{kT}{q}\right) \quad (5)$$

where N_A and N_D are the acceptor and donor density in the passive film respectively, E is the applied potential, E_{FB} is the flat band potential, k is the Boltzman constant ($1.38 \cdot 10^{-23}$ J/K), T is the absolute temperature and q is the electron charge ($1.6 \cdot 10^{-19}$ C), ε_0 is the vacuum permittivity ($8.85 \cdot 10^{-14}$ F cm^{-1}) and ε denotes the relative dielectric constant of the layer.

Therefore, the validity of the M-S analysis is based on the assumption that the capacitance of the space-charge layer is much lower than that of the Helmholtz layer [85] and the data points on the $1/C_{SC}^2$ versus E plot can describe the semiconductive behaviour of the depletion region. N_A and N_D can be determined from the slope of this experimental data.

Figure 8 presents M-S curves for the passive films formed on Alloy 31 at 0.8 $V_{Ag/AgCl}$ in the phosphoric acid solution at different temperatures. Firstly, it should be noted that capacitance clearly increases with temperature, which is consistent with the results of the polarisation curves and EIS measurements. In the potential range of around 0.2-0.7

$V_{Ag/AgCl}$, a linear relationship can be observed between C^{-2} and E at the four temperatures. Within this potential range, the positive slopes suggest all the passive films formed on Alloy 31 are of an n-type semiconductor nature. Below 0.2 $V_{Ag/AgCl}$ the slope of the M-S curves is close to zero.

According to equation (5), N_D can be determined from the slope of the experimental M-S plots, and E_{FB} from the extrapolation of the linear portion to $C^{-2} = 0$. Because the slope is inversely proportional to the donor density, the decrease in the slope when temperature increases indicates that the concentration of donor species in the passive film increases with temperature [79], which implies that high donor densities lead to high current density values in the passive region. This observation is consistent with the results obtained from the polarisation curves and the current density-time transients. **Table 6** summarises the calculated donor densities for the films formed on Alloy 31 and they are all of the order of 10^{21} cm^{-3}, which agree well with those reported for austenitic stainless steels [8, 67, 82, 86]. The higher donor density values at elevated temperatures means that the passive film on Alloy 31 has higher electron density and lower impedance, as observed in the EIS measurements. All these statements confirm that the protective ability of the passive films formed on Alloy 31 decreases with increase in temperature. The aggressive ions, Cl^- and F^- have a great influence on the stability of the passive films.

3.6. XPS results

XPS analysis was undertaken to provide additional information on the chemical composition of the passive films. The XPS spectra were obtained for the samples

passivated at 0.8 $V_{Ag/AgCl}$ in phosphoric acid solutions at different temperatures. **Figure 9** shows a typical wide scan spectrum from the surface of a treated alloy, belonging to the sample treated at 80 ºC. **Table 7** summarises the surface elemental concentration (% atomic concentration) of each sample analysed. There is clearly a decrease in carbon concentration with increasing temperature which may be evidence that the surface is dissolving more rapidly. Moreover, these results indicate that there is increasing fluorine incorporation into the surface with temperature, which is an indication that fluoride ions are incorporated into the passive film and, as a consequence, the passive film is more susceptible to damage.

The surface concentrations of the principal alloying elements have been renormalized to illustrate any trend and are shown in **Table 8**. There is an indication of increasing Ni and decreasing Cr within the film with increasing temperature while molybdenum content hardly changes. The decrease in chromium atomic concentration may be attributed to the fact temperature favours the dissolution of these species. On the other hand, as the role of Ni and Mo in stainless steels at anodic potentials in acid solutions is to stabilise the passive film and to eliminate the active surface sites [87], the increase in temperature hardly changes its atomic concentration on the passive film.

The XPS spectra were interpreted following background subtraction using the *CasaXPS* software and spectra deconvolution of the primary compounds of Alloy 31 passive film were prepared with the corresponding peaks of each element based on their binding energies *(E_b)*. Peak fitting was carried out on the high energy resolved data where overlapping photoelectron peaks occur, to determine the chemical state of the species

present in the passive film. Next figures present all of the metallic and oxidised states of Ni 2p, Mo 3d, Fe 2p and Cr 2p.

The Ni 2p high resolution data were compared, and apart from differences in background and intensity appeared to have similar shapes. Peak fitting was carried out to the $2p_{3/2}$ region of the most intense spectrum, from the 80 ºC treatment, and it is shown in **Figure 10**. The envelope labelled Ni1 is composed of three peaks, fited to reference data [88], and constitutes elemental Ni. The envelope labelled Ni2 is again composed of three peaks and is most likely NiOOH [89]. Note that the principal Ni $2p_{3/2}$ peak for Ni_2O_3 apears at 860.9 eV binding energy [90], and the principal peak for NiO occurs at 855.4 eV and shows significant satellite structure [88].

This peak fit was applied to the Ni $2p_{3/2}$ data for all temperatures whilst constraining the relative intensities of the peaks within each component, and the relative intensities of Ni and NiOOH are shown in **Table 9**. No significant trend can be seen on changing the treatment temperature.

Inspection of the Mo 3d high resolution data in **Figure 11** also showed similar peak envelopes once backgrounds and intensity had been taken into consideration. Peak fitting was carried out across the entire 3d region and the spin orbit components were constrained with a separation of 3.1 eV and a 3/2:1/2 peak area intensity of 3:2. A spectrum was acquired from a clean molybdenum surface and used for the elemental molybdenum component, labelled Mo 0. A pair of peaks for each spin orbit split component was fitted for MoO_2, Mo 1 and Mo 2. The low binding energy, narrow FWHM, for the screened peak, Mo 1-1, results in the conductive nature of this oxide

[91]. A pair of peaks labelled Mo 2 was fitted to and assigned as MoO_3. It was then necessary to add a spin orbit split pair with the $3d_{5/2}$ peak at 231.2 eV binding energy, which may be a fluoride, MoF_4, although malybdate, $(MoO_4)^{2-}$, is more likely.

Due to the strong acidic conditions in this electrolyte (pH < 1), the presence of MoO_3 was expected, since these conditions lead to the formation of this insoluble oxide [92], which is responsible for the n-type semiconducting behaviour [93, 94] observed in the previous M-S section.

The peak fit was applied to the Mo 3d data for all temperatures, and the relative intensities of the different chemical states do not show any trend with increasing temperature (values in **Table 9**).

Figure 12 shows the high energy resolution Fe 2p data, which was fitted using multiplet split components to determine the elemental, Fe^{2+} and Fe^{3+} components [95]. Analysis of these data is summarised in **Table 9**, giving the relative intensities of each component. The data does not show any discernable trend with changing temperature.

Finally, peak fitting to the Cr $2p_{3/2}$ region is presented in **Figure 13**, using the peak parameters of Biesinger [96] for Cr 0, Cr 1 and Cr 3 peaks.

Cr 0 represents chromium metal, Cr 1 is $Cr(OH)_3$, and Cr 3 is CrO_3. Cr_2O_3 would have principal peaks at 575.7 eV and 576.7 eV [96]. Peak Cr 1 has been designed to incorporate the multiplet splitting exhibited by the Cr(III) state. Peak Cr 2 is possibly a

chromate species, $(CrO_4)^2$. The relative intensities of these peaks applied to the data at different temperatures are shown in **Table 9**.

4. CONCLUSIONS

The electrochemical behaviour of passive film formed on Alloy 31 stainless steel in a contaminated phosphoric acid solution has been investigated using potentiodynamic polarisation curves, current-time transients, EIS, M-S analysis and XPS.

The polarisation curves revealed that the corrosion potential (E_{corr}) shifted towards more positive values and corrosion current density (i_{corr}) values increased with increasing temperature, due to the enhancement of the cathodic reaction when temperature increases. Passive current density (i_p) increased with increasing temperature, since temperature also favours the anodic process and the presence of the aggressive ions accelerates the anodic dissolution, leading to the loss of passivity of Alloy 31. This fact was reflected in the transpassive potential (E_{tr}) values, which decreased as solution temperature increased.

The passive film formed on Alloy 31 at lower temperatures has a superior protective ability than that formed at higher temperatures. It was demonstrated that the passivation index, *n* slightly decreased as temperature increases.

EIS measurements showed that impedance is dependent on the temperature. But in all cases, the protection provided by the passive film was predominantly due to the inner oxide film. The increase in temperature indicated higher electrical conductivity on the

passive film formed on Alloy 31 and thinner films as a result of higher capacitance values.

Mott-Schottky analysis revealed the films formed exhibited an n-type semiconducting behaviour. Donor density values were of the order of 10^{21} cm^{-3}, and tended to increase with temperature, indicating higher electron density.

XPS analysis revealed that fluoride ions were incorporated into the passive film, increasing its atomic concentration as temperature increases. This, along with the reduction of chromium species reflects a reduction in passive film stability.

Acknowledgements.

Authors express their gratitude to the Ministry of Education of Spain (MHE2011-00202) for its financial support during the stay at University of Manchester, to MAEC of Spain (PCI Mediterráneo C/8196/07, C/018046/08, D/023608/09 and D/030177/10) and to the Generalitat Valenciana (GV/2011/093) for the financial support. The authors would also like to acknowledge the support of the School of Materials at the University of Manchester for providing analytical and technical support for the study.

References

[1] B. Lochel, H. H. Strehblow, M. Sakashita, Breakdown of passivity of nickel by fluoride.1.Electrochemical studies, Journal of the Electrochemical Society 131 (1984) 522.

[2] I. Sekine, H. Usui, S. Kitagawa, M. Yuasa, L. Silao, The effect of fluoride ions on the corrosion of steel materials in H_2SO_4 and CH_3COOH solutions, Corrosion Science 36 (1994) 1411.

[3] J. M. Bastidas, C. Fosca, B. Chico, E. Otero, Weight loss and electrochemical results for two super-austenitic stainless steels in chloride-fluoride mixtures, Corrosion Science 38 (1996) 559.

[4] J. B. Lee, Effects of alloying elements, Cr, Mo and N on repassivation characteristics of stainless steels using the abrading electrode technique, Materials Chemistry and Physics 99 (2006) 224.

[5] G. T. Burstein, B. T. Daymond, The remarkable passivity of austenitic stainless steel in sulphuric acid solution and the effect of repetitive temperature cycling, Corrosion Science 51 (2009) 2249.

[6] B. Jegdic, D. M. Drazic, J. P. Popic, Corrosion potential of 304 stainless steel in sulfuric acid, Journal of the Serbian Chemical Society 71 (2006) 543.

[7] D. A. Jones, N. D. Greene, Electrochemical measurement of low corrosion rates, Corrosion 22 (1966) 198.

[8] K. S. Raja, D. A. Jones, Effects of dissolved oxygen on passive behavior of stainless alloys, Corrosion Science 48 (2006) 1623.

[9] B. Stypula, D. Kasprzyk, M. Hajos, Corrosion behaviour of stainless steel in hot concentrated sulfuric acid: Effect of fluoride impurities, Archives of Metallurgy and Materials 54 (2009) 305.

[10] H. Iken, R. Basseguy, A. Guenbour, A. B. Bachir, Classic and local analysis of corrosion behaviour of graphite and stainless steels in polluted phosphoric acid, Electrochimica Acta 52 (2007) 2580.

[11] A. Guenbour, M. A. Hajji, E. M. Jallouli, A. B. Bachir, Study of corrosion-erosion behaviour of stainless alloys in industrial phosphoric acid medium, Applied Surface Science 253 (2006) 2362.

[12] A. Bellaouchou, A. Guenbour, A. Benbachir, The corrosion of an austenetic stainless steel in phosphoric acid: Effect of sulphide ions and abrasive action, Bulletin of Electrochemistry 16 (2000) 166.

[13] C. Escrivà-Cerdán, E. Blasco-Tamarit, D. M. García-García, J. García-Antón, A. Guenbour, Passivation behaviour of Alloy 31 (UNS N08031) in polluted phosphoric acid at different temperatures, Corrosion Science 56 (2012) 114.

[14] M. C. Li, C. L. Zeng, H. C. Lin, C. N. Cao, Electrochemical corrosion behaviour of type 316 stainless steel in acid media containing fluoride ions, British Corrosion Journal 36 (2001) 179.

[15] J. M. Bastidas, C. Fosca, B. Chico, E. Otero, Corrosion behaviour of highly alloyed stainless steels in mixed chloride and fluoride aqueous solutions, Materials and Corrosion 48 (1997) 26.

[16] Pierre Becker, Phosphates and phosphoric acid. Raw materials, technology, and economics of the wet process, M. Dekker (eds.), New York, 1989.

[17] ASTM G-5. Test Method for Making Potentiostatic and Potentiodynamic Anodic Polarization Measurements. American Society for Testing and Materials. 2004.

[18] Y. X. Qiao, Y. G. Zheng, W. Ke, P. C. Okafor, Electrochemical behaviour of high nitrogen stainless steel in acidic solutions, Corrosion Science 51 (2009) 979.

[19] N. Li, Y. Li, S. Wang, F. Wang, Electrochemical corrosion behavior of nanocrystallized bulk 304 stainless steel, Electrochimica Acta 52 (2006) 760.

[20] Y. X. Qiao, Y. G. Zheng, P. C. Okafor, W. Ke, Electrochemical behaviour of high nitrogen bearing stainless steel in acidic chloride solution: Effects of oxygen, acid concentration and surface roughness, Electrochimica Acta 54 (2009) 2298.

[21] Walton J., Fairley N., A traceable quantification procedure for a multi-mode X-ray photoelectron spectrometer, Journal of Electron Spectroscopy and Related Phenomena 150 (2006) 15.

[22] E. A. Abd El Meguid, A. A. Abd El Latif, Critical pitting temperature for Type 254 SMO stainless steel in chloride solutions, Corrosion Science 49 (2007) 263.

[23] G. Lothongkum, S. Chaikittisilp, A. W. Lothongkum, XPS investigation of surface films on high Cr-Ni ferritic and austenitic stainless steels, Applied Surface Science 218 (2003) 203.

[24] E. Blasco-Tamarit, A. Igual-Muñoz, J. García Antón, D. García-García, Effect of temperature on the corrosion resistance and pitting behaviour of Alloy 31 in LiBr solutions, Corrosion Science 50 (2008) 1848.

[25] L. F. Garfias-Mesias, J. M. Sykes, Metastable pitting in 25 Cr duplex stainless steel, Corrosion Science 41 (1999) 959.

[26] A. Igual Muñoz, J. García Antón, S. López Nuévalos, J. L. Guiñón, V. Pérez Herranz, Corrosion studies of austenitic and duplex stainless steels in aqueous lithium bromide solution at different temperatures, Corrosion Science 46 (2004) 2955.

[27] N. J. Laycock, Effects of temperature and thiosulfate on chloride pitting of austenitic stainless steels, Corrosion 55 (1999) 590.

[28] A. Pardo, E. Otero, M. C. Merino, M. D. Lopez, M. V. Utrilla, F. Moreno, Influence of pH and chloride concentration on the pitting and crevice corrosion behavior of high-alloy stainless steels, Corrosion 56 (2000) 411.

[29] D. H. Hur, Y. S. Park, Effect of temperature on the pitting behavior and passive film characteristics of alloy 600 in chloride solution, Corrosion 62 (2006) 745.

[30] A. Igual-Muñoz, J. García-Antón, J. L. Guiñón, V. Pérez-Herranz, Effects of solution temperature on localized corrosion of high nickel content stainless steels and nickel in chromated LiBr solution, Corrosion Science 48 (2006) 3349.

[31] C. O. A. Olsson, D. Landolt, Passive films on stainless steels--chemistry, structure and growth, Electrochimica Acta 48 (2003) 1093.

[32] A. Guenbour, H. Iken, N. Kebkab, A. Bellaouchou, R. Boulif, A. B. Bachir, Corrosion of graphite in industrial phosphoric acid, Applied Surface Science 252 (2006) 8710.

[33] M. Ibáñez-Ferrándiz, M. Blasco-Tamarit, D. M. García-García, J. García-Antón, A. Guenbour, S. Bakour, A. Benckokroun, Effect of temperature on the corrosion resistance of stainless steels in polluted phosphoric acid, ECS Transactions 25 (2010) 49.

[34] M. V. Cardoso, S. T. Amaral, E. M. A. Martini, Temperature effect in the corrosion resistance of Ni-Fe-Cr alloy in chloride medium, Corrosion Science 50 (2008) 2429.

[35] S. Zor, M. Soncu, L. Ãapan, Corrosion behavior of G-X CrNiMoNb 18-10 austenitic stainless steel in acidic solutions, Journal of Alloys and Compounds 480 (2009) 885.

[36] A. M. M. Ibrahim, S. S. Abd El Rehim, M. M. Hamza, Corrosion behavior of some austenitic stainless steels in chloride environments, Materials Chemistry and Physics 115 (2009) 80.

[37] E. Blasco-Tamarit, D. M. García-García, J. García-Antón, Imposed potential measurements to evaluate the pitting corrosion resistance and the galvanic behaviour of a highly alloyed austenitic stainless steel and its weldment in a LiBr solution at temperatures up to 150 ºC, Corrosion Science 53 (2011) 784.

[38] A. Neville, T. Hodgkiess, An assessment of the corrosion behaviour of high-grade alloys in seawater at elevated temperature and under a high velocity impinging flow, Corrosion Science 38 (1996) 927.

[39] M. Drogowska, H. Menard, L. Brossard, Electrooxidation of stainless steel AISI 304 in carbonate aqueous solution at pH8, Journal of Applied Electrochemistry 26 (1996) 217.

[40] M. Drogowska, L. Brossard, H. Menard, 304 stainless steel oxidation in sulfate and sulfate plus bicarbonate solutions, Journal of Applied Electrochemistry 28 (1998) 491.

[41] H. Wang, J. A. Turner, Austenitic stainless steels in high temperature phosphoric acid, Journal of Power Sources 180 (2008) 803.

[42] M. Reffass, R. Sabot, M. Jeannin, C. Berziou, P. Refait, Effects of phosphate species on localised corrosion of steel in $NaHCO_3$+NaCl electrolytes, Electrochimica Acta 54 (2009) 4389.

[43] S. R. Moraes, D. Huerta-Vilca, A. J. Motheo, Corrosion protection of stainless steel by polyaniline electrosynthesized from phosphate buffer solutions, Progress in Organic Coatings 48 (2003) 28.

[44] H. Bouchemel, A. Benchettara, Corrosion behaviour of Ti40Cu60 alloy in H_3PO_4 solutions, Materials Chemistry and Physics 115 (2009) 572.

[45] R. Sánchez-Tovar, M. T. Montañés, J. García-Antón, The effect of temperature on the galvanic corrosion of the copper/AISI 304 pair in LiBr solutions under hydrodynamic conditions, Corrosion Science 52 (2010) 722.

[46] M. Lakatos-Varsányi, F. Falkenberg, I. Olefjord, The influence of phosphate on repassivation of 304 stainless steel in neutral chloride solution, Electrochimica Acta 43 (1998) 187.

[47] G. O. Ilevbare, G. T. Burstein, The role of alloyed molybdenum in the inhibition of pitting corrosion in stainless steels, Corrosion Science 43 (2001) 485.

[48] J. d. Kim, S. i. Pyun, Effects of electrolyte composition and applied potential on the repassivation kinetics of pure aluminium, Electrochimica Acta 40 (1995) 1863.

[49] S. i. Pyun, E. J. Lee, Effect of halide ion and applied potential on repassivation behaviour of Al-1 wt.%Si-0.5 wt.%Cu alloy, Electrochimica Acta 40 (1995) 1963.

[50] R. M. Fernández-Domene, E. Blasco-Tamarit, D. M. García-García, J. García-Antón, Repassivation of the damage generated by cavitation on UNS N08031

in a LiBr solution by means of electrochemical techniques and Confocal Laser Scanning Microscopy, Corrosion Science 52 (2010) 3453.

[51] J. J. Park, S. I. Pyun, W. J. Lee, H. P. Kim, Effect of bicarbonate ion additives on pitting corrosion of type 316L stainless steel in aqueous 0.5 M sodium chloride solution, Corrosion 55 (1999) 380.

[52] H. H. Hassan, Effect of chloride ions on the corrosion behaviour of steel in 0.1M citrate, Electrochimica Acta 51 (2005) 526.

[53] J. R. Galvele, R. M. Torresi, R. M. Carranza, Passivity breakdown, its relation to pitting and stress-corrosion-cracking processes, Corrosion Science 31 (1990) 563.

[54] Z. Szklarska-Smialowska, Pitting corrosion of aluminum, Corrosion Science 41 (1999) 1743.

[55] A. Pardo, M. C. Merino, A. E. Coy, F. Viejo, R. Arrabal, E. Matykina, Pitting corrosion behaviour of austenitic stainless steels - combining effects of Mn and Mo additions, Corrosion Science 50 (2008) 1796.

[56] B. Evgenij, R. M. J, Impedance Spectroscopy: Theory, Experiment and Applications, West Sussex, UK, 2005.

[57] M. Urquidi-Macdonald, S. Real, D. D. Macdonald, Application of Kramers-Kronig Transforms in the analysis of electrochemical impedance data, Journal of the Electrochemical Society 133 (1986) 2018.

[58] M. Urquidi-Macdonald, S. Real, D. D. Macdonald, Applications of Kramers-Kronig transforms in the analysis of electrochemical impedance data. III. Stability and linearity, Electrochimica Acta 35 (1990) 1559.

[59] G. J. Brug, A. L. G. Vandeneeden, M. Sluytersrehbach, J. H. Sluyters, The analysis of alectrode impedances complicated by the presence of a constant phase element, Journal of Electroanalytical Chemistry 176 (1984) 275.

[60] F. B. Growcock, J. H. Jasinski, Time-resolved impedance spectroscopy of mild-stel in concentrated hydrochloric acid, Journal of the Electrochemical Society 136 (1989) 2310.

[61] R. Fuchs-Godec, M. G. Pavlovic, Synergistic effect between non-ionic surfactant and halide ions in the forms of inorganic or organic salts for the corrosion inhibition of stainless-steel X4Cr13 in sulphuric acid, Corrosion Science 58 (2012) 192.

[62] S. L. d. Assis, S. Wolynec, I. Costa, Corrosion characterization of titanium alloys by electrochemical techniques, Electrochimica Acta 51 (2006) 1815.

[63] J. Pan, C. Leygraf, R. F. A. Jargelius-Pettersson, J. Linden, Characterization of high-temperature oxide films on stainless steels by electrochemical-impedance spectroscopy, Oxidation of Metals 50 (1998) 431.

[64] K. Jüttner, Electrochemical impedance spectroscopy (EIS) of corrosion processes on inhomogeneous surfaces, Electrochimica Acta 35 (1990) 1501.

[65] S. Yagi, A. Sengoku, K. Kubota, E. Matsubara, Surface modification of ACM522 magnesium alloy by plasma electrolytic oxidation in phosphate electrolyte, Corrosion Science 57 (2012) 74.

[66] C. Escrivà-Cerdán, E. Blasco-Tamarit, D. García-García, J. García-Antón, A. Guenbour, Effect of potential formation on the electrochemical behaviour of a highly alloyed austenitic stainless steel in contaminated phosphoric acid at different temperatures, Electrochimica Acta 80 (2012) 248.

[67] M. Metikos-Hukovic, R. Babic, Z. Grubac, Z. Petrovic, N. Lajci, High corrosion resistance of austenitic stainless steel alloyed with nitrogen in an acid solution, Corrosion Science 53 (2011) 2176.

[68] H. Huan, Z. Tao, Z. Chengzhi, H. Kai, M. Gouzhe, S. Yawei, W. Fuhui, Effect of alternating voltage passivation on the corrosion resistance of duplex stainless steel, Journal of Applied Electrochemistry 39 (2009) 737.

[69] N. P. Cosman, K. Fatih, S. G. Roscoe, Electrochemical impedance spectroscopy study of the adsorption behaviour of a-lactalbumin and b-casein at stainless steel, Journal of Electroanalytical Chemistry 574 (2005) 261.

[70] K. C. Emregül, A. A. Aksüt, The behavior of aluminum in alkaline media, Corrosion Science 42 (2000) 2051.

[71] D. D. Macdonald, Review of mechanistic analysis by electrochemical impedance spectroscopy, Electrochimica Acta 35 (1990) 1509.

[72] J. B. Bessone, D. R. Salinas, C. E. Mayer, M. Ebert, W. J. Lorenz, An EIS study of aluminium barrier-type oxide films formed in different media, Electrochimica Acta 37 (1992) 2283.

[73] O. R. Brown, J. S. Whitley, Electrochemical behaviour of aluminium in aqueous caustic solutions, Electrochimica Acta 32 (1987) 545.

[74] M. Metikos-Hukovic, Z. Pilic, R. Babic, D. Omanovic, Influence of alloying elements on the corrosion stability of CoCrMo implant alloy in Hank's solution, Acta Biomaterialia 2 (2006) 693.

[75] A. Kocijan, D. K. Merl, M. Jenko, The corrosion behaviour of austenitic and duplex stainless steels in artificial saliva with the addition of fluoride, Corrosion Science 53 (2011) 776.

[76] R. M. Fernández-Domene, E. Blasco-Tamarit, D. M. García-García, J. García-Antón, Thermogalvanic corrosion of Alloy 31 in different heavy brine LiBr solutions, Corrosion Science 55 (2012) 40.

[77] Y. B. Hu, C. F. Dong, M. Sun, K. Xiao, P. Zhong, X. G. Li, Effects of solution pH and Cl- on electrochemical behaviour of an Aermet100 ultra-high strength steel in acidic environments, Corrosion Science 53 (2011) 4159.

[78] G. Goodlet, S. Faty, S. Cardoso, P. P. Freitas, A. M. P. Simoes, M. G. S. Ferreira, M. Cunha Belo, The electronic properties of sputtered chromium and iron oxide films, Corrosion Science 46 (2004) 1479.

[79] M. J. Carmezim, A. M. Simoes, M. F. Montemor, M. D. Cunha Belo, Capacitance behaviour of passive films on ferritic and austenitic stainless steel, Corrosion Science 47 (2005) 581.

[80] L. Liu, Y. Li, F. Wang, Influence of nanocrystallization on passive behavior of Ni-based superalloy in acidic solutions, Electrochimica Acta 52 (2007) 2392.

[81] D. D. Macdonald, The Point Defect Model for the passive state, Journal of the Electrochemical Society 139 (1992) 3434.

[82] A. Di Paola, Semiconducting properties of passive films on stainless steels, Electrochimica Acta 34 (1989) 203.

[83] R. Degryse, W. P. Gomes, F. Cardon, J. Vennik, Interpretation of Mott-Schottky Plots Determined at Semiconductor-Electrolyte Systems, Journal of the Electrochemical Society 122 (1975) 711.

[84] B. Pettinge, HR. Schoppel, T. Yokoyama, H. Gerische, Tunnelling processes at highly doped ZnO-electrodes in aqueous electrolytes. 2. Electron exchange with valence band, Berichte der Bunsen-Gesellschaft Physical Chemistry Chemical Physics 78 (1974) 1024.

[85] N. E. Hakiki, M. D. Belo, A. M. P. Simoes, M. G. S. Ferreira, Semiconducting properties of passive films formed on stainless steels - Influence of the alloying elements, Journal of the Electrochemical Society 145 (1998) 3821.

[86] F. Gaben, B. Vuillemin, R. Oltra, Influence of the chemical composition and electronic structure of passive films grown on 316L SS on their transient

electrochemical behavior, Journal of the Electrochemical Society 151 (2004) B595.

[87] H. Iken, R. Basseguy, A. Guenbour, A.B. Bachir, Classic and local analysis of corrosion behaviour of graphite and stainless steels in polluted phosphoric acid, Electrochimica Acta 52 (2007) 2580.

[88] M. C. Biesinger, B. P. Payne, L.W.M. Lau, A. Gerson, R.S.C Smart, X-ray photoelectron spectroscopic chemical state quantification of mixed nickel metal, oxide and hydroxide systems, Surface and Interface Analysis 41 (2009) 324.

[89] A.P Grosvenor, M. C. Biesinger, RS. Smart, NS McIntyre, New interpretations of XPS spectra of nickel metal and oxides, Surface Science, 600 (2006) 1771.

[90] A. N. Mansour, C. A. Melendres, Characterization of $Ni_2O_3 \cdot 6H_2O$ by XPS, Surface Science Spectra, 3 (1994) 263.

[91] D. O. Scanlon, G. W. Watson, D. J. Payne, G. R. Atkinson, R. G. Egdell, D. S. L. Law, Theoretical and Experimental Study of the Electronic Structures of MoO_3 and MoO_2, Journal of Physical Chemistry C 114 (2010) 4636.

[92] A. Pardo, M. C. Merino, A. E. Coy, F. Viejo, R. Arrabal, E. Matykina, Effect of Mo and Mn additions on the corrosion behaviour of AISI 304 and 316 stainless steels in H_2SO_4, Corrosion Science 50 (2008) 780.

[93] C. Sunseri, S. Piazza, F. Di Quarto, Photocurrent spectroscopy investigations of passive films on chromium, Journal of the Electrochemical Society 137 (1990) 2411.

[94] M. H. Dean, U. Stimming, The electronic properties of disordered passive films, Corrosion Science 29 (1989) 199.

[95] NS. McIntyre, D. G. Zetaruk, X-ray photoelectron spectroscopic studies of iron-oxides, Analytical Chemistry 49 (1977) 1521.

[96] M. C. Biesinger, B. P. Payne, A. P. Grosvenor, L. W. M. Lau, A. R. Gerson, R. S. C. Smart, Resolving surface chemical states in XPS analysis of first row transition metals, oxides and hydroxides: Cr, Mn, Fe, Co and Ni, Applied Surface Science 257 (2011) 2717.

Table 1. Chemical composition of the UNS N08031 (Alloy 31) (wt.%).

	%Cr	**%Fe**	**%Ni**	**%Mo**	**%Mn**	**%Cu**	**%N**	**%Si**	**%C**	**%S**	**%P**
Alloy 31	26.75	31.43	31.85	6.6	1.5	1.21	0.193	0.1	0.005	0.002	0.017

Table 2. OCP values for Alloy 31 in the studied H_3PO_4 solution at different temperatures.

Temperature / ºC	20	40	60	80
OCP / mV$_{Ag/AgCl}$	220.4	277.3	302.2	320.1

Table 3. Electrochemical parameters for Alloy 31 in the studied H_3PO_4 solution at different temperatures.

t / °C	**E_{corr} vs (Ag/AgCl) / mV**	**i_{corr} / μA·cm^{-2}**	**i_p / μA·cm^{-2}**	**E_{tr} vs (Ag/AgCl) / mV**
20	235	1.306	7.35	1142
40	289	1.192	12.6	1124
60	326	2.073	26.0	969
80	375	6.705	46.0	771

Table 4. Stable state current density i_{ss} and passivation parameter n for Alloy 31 in the studied H_3PO_4 solution at different temperatures after 1 hour of stabilisation of passive films at 0.8 $V_{Ag/AgCl}$.

t / ºC	**(i_{ss} · 10^3) / mA·cm^{-2}**	***n***
20	5.04	0.78
40	21.7	0.78
60	63.1	0.76
80	143	0.61

Table 5. Electrical parameters obtained by fitting the experimental results of EIS for Alloy 31 in the contaminated phosphoric acid solution at different temperatures after passive film formation at 0.8 $V_{Ag/AgCl}$.

t / ºC	R_S / Ω cm^2	α_1	R_1 / KΩ cm^2	C_1 / μF·cm^{-2}	α_2	R_2 / KΩ cm^2	C_2 / μF·cm^{-2}	
20	1.20	0.920	3.16	15.9	0.857	14.8	32.4	
t / ºC		**α_1**	**R_1 / KΩ cm^2**	**C_1 / μF·cm^{-2}**	**α_2**	**R_2 / KΩ cm^2**	**C_2 / μF·cm^{-2}**	**R_L / KΩ cm^2**
40	1.01	0.917	0.89	15.0	0.600	3.12	36.89	0.84
60	1.37	0.891	1.55	19.3	1.000	2.84	27374	0.14
80	1.28	0.906	0.99	16.5	0.949	2.62	18590	0.10

Table 6. Donor density, N_D and flat band potentials, E_{FB} of the oxide films formed on Alloy 31 at 0.8 $V_{Ag/AgCl}$ and at different temperatures.

t / ºC	**(N_D/10^{21}) / cm^{-3}**	**E_{FB} vs (Ag/AgCl) / V**
20	2.77	-0.465
40	3.16	-0.491
60	3.68	-0.441
80	5.46	-0.751

Table 7. Surface elemental compositions (% atomic concentration) of the passive films formed on Alloy 31 after 1 hour of stabilisation under 0.8 $V_{Ag/AgCl}$ and different temperatures.

t / ºC	Fe (%ac)	Cr (%ac)	Ni (%ac)	O (%ac)	F (%ac)	C (%ac)	Mo (%ac)	S (%ac)	Si (%ac)	P (%ac)
20	1.5	3.5	1.3	28.1	2.6	56.2	0.7	2.1	3.6	0.6
40	2.3	6.5	3.0	32.4	4.5	41.1	1.0	2.9	5.4	0.8
60	3.2	5.1	3.5	32.1	4.6	45.0	1.1	1.6	2.8	1.0
80	35	6.3	3.2	34.3	6.5	39.0	1.4	1.7	2.8	1.5

Table 8. Renormalized surface compositions of the principal alloying elements (% atomic concentrations).

t / ºC	Fe (%ac)	Cr (%ac)	Ni (%ac)	Mo (%ac)
20	21.4	50.0	18.6	10.0
40	18.0	50.8	23.4	7.8
60	24.8	39.5	27.1	8.5
80	24.3	43.8	22.2	9.7

Table 9. Relative intensities of the peaks within each component detected on Alloy 31 surface after 1 h of polarisation at 0.8 $V_{Ag/AgCl}$ and at different temperatures.

Species	20 ºC	40 ºC	60 ºC	80 ºC
Ni	72.0	74.2	77.1	71.1
NiOOH	28.0	25.8	23.0	29.0
Mo	16.4	17.7	16.8	16.4
MoO_2	20.8	17.8	19.5	21.8
$(MoO_4)^{2-}$	17.5	14.3	19.9	19.2
MoO_3	45.3	50.3	43.8	42.6
Fe^0	34.2	35.0	34.8	36.3
Fe^{2+}	39.8	36.0	31.7	37.6
Fe^{3+}	26.0	29.0	33.6	26.1
Cr	19.2	18.3	26.9	28.3
$Cr(OH)_3$	50.1	48.0	37.7	21.5
$(CrO_4)^{2-}$	25.2	27.9	30.8	41.2
CrO_3	5.5	5.8	4.6	9.0

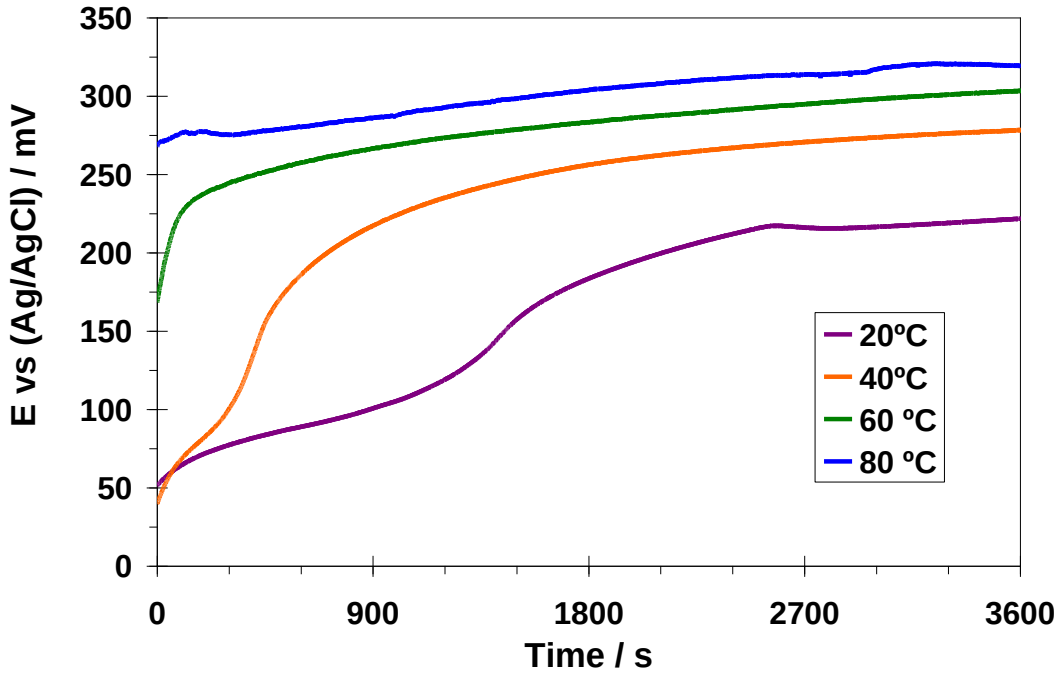

Figure 1. Evolution of the open circuit potential with time for the Alloy 31 registered during 1 hour at 20, 40, 60 and 80 ºC in 40 wt.% polluted phosphoric acid solution.

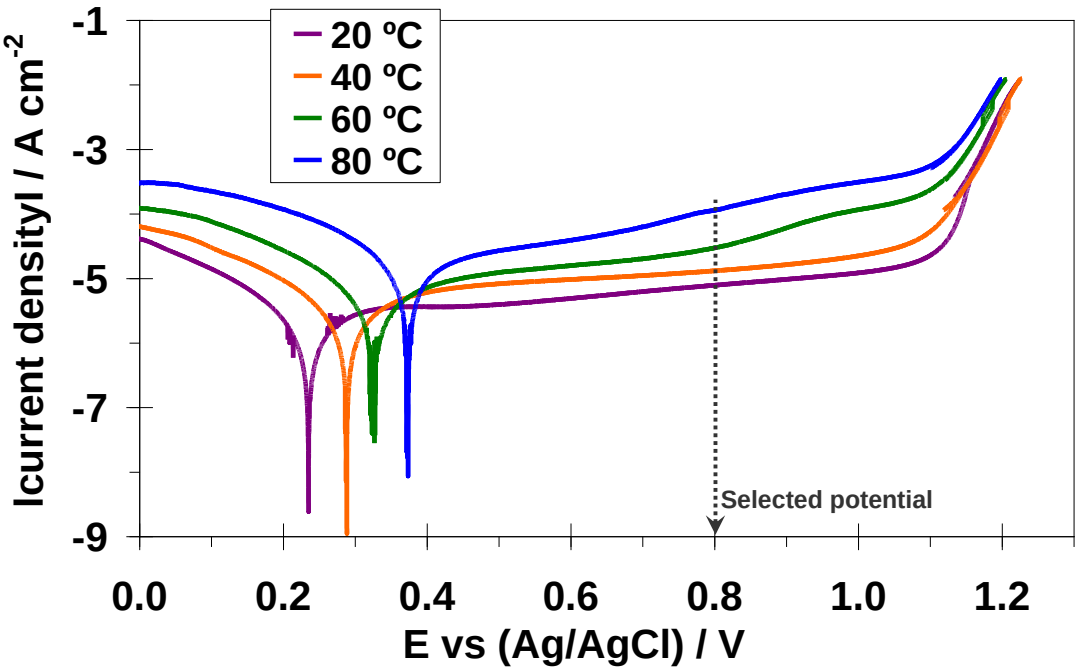

Figure 2. Potentiodynamic curves of Alloy 31 in polluted 40 wt.% H_3PO_4 with 2 wt.% H_2SO_4, 0.06 wt.% KCl and 0.6 wt.% HF at different temperatures.

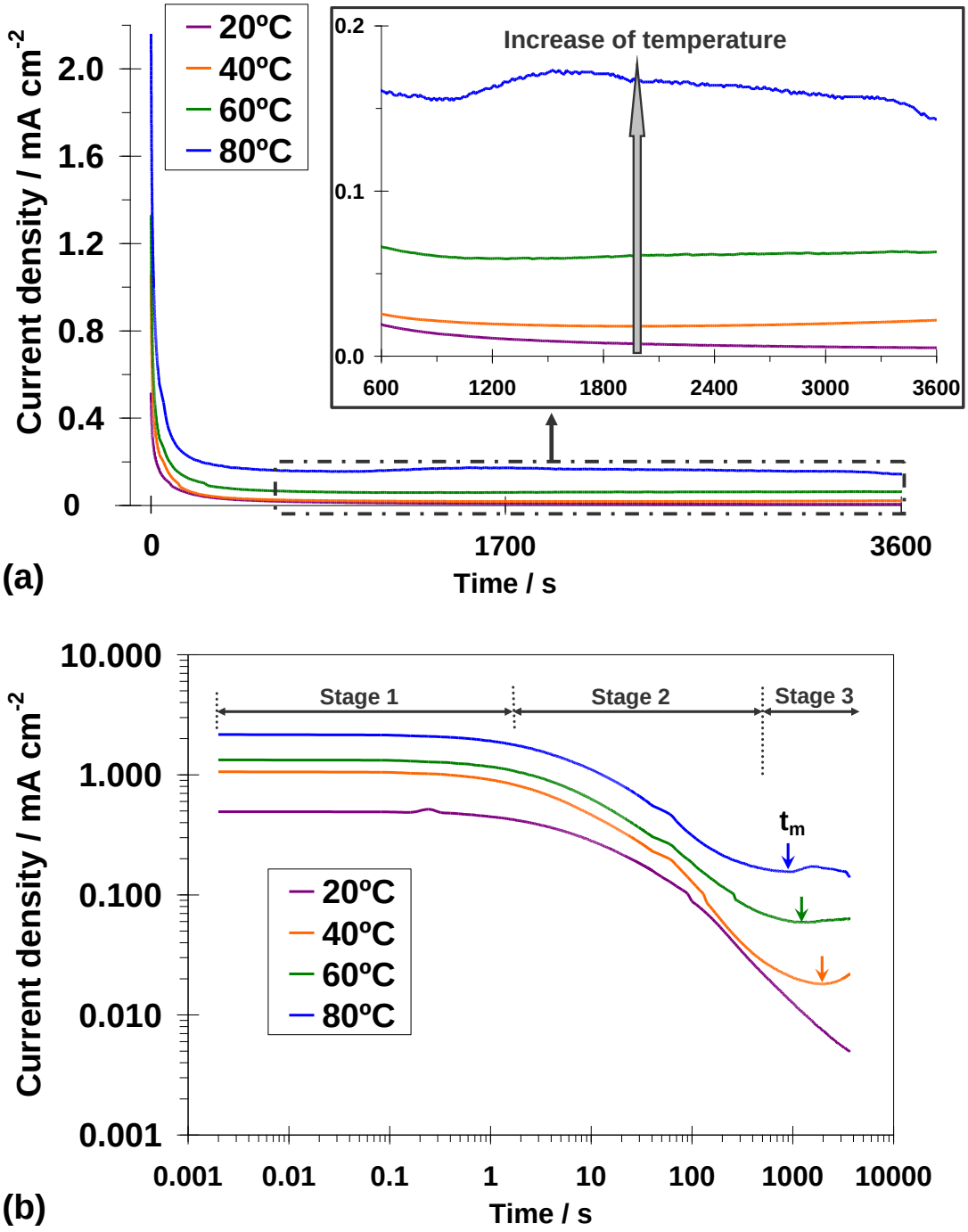

Figure 3. (a) Current-time transients and **(b)** *log i-log t* plots of current time for Alloy 31 in the contaminated phosphoric acid solution at the different temperatures studied.

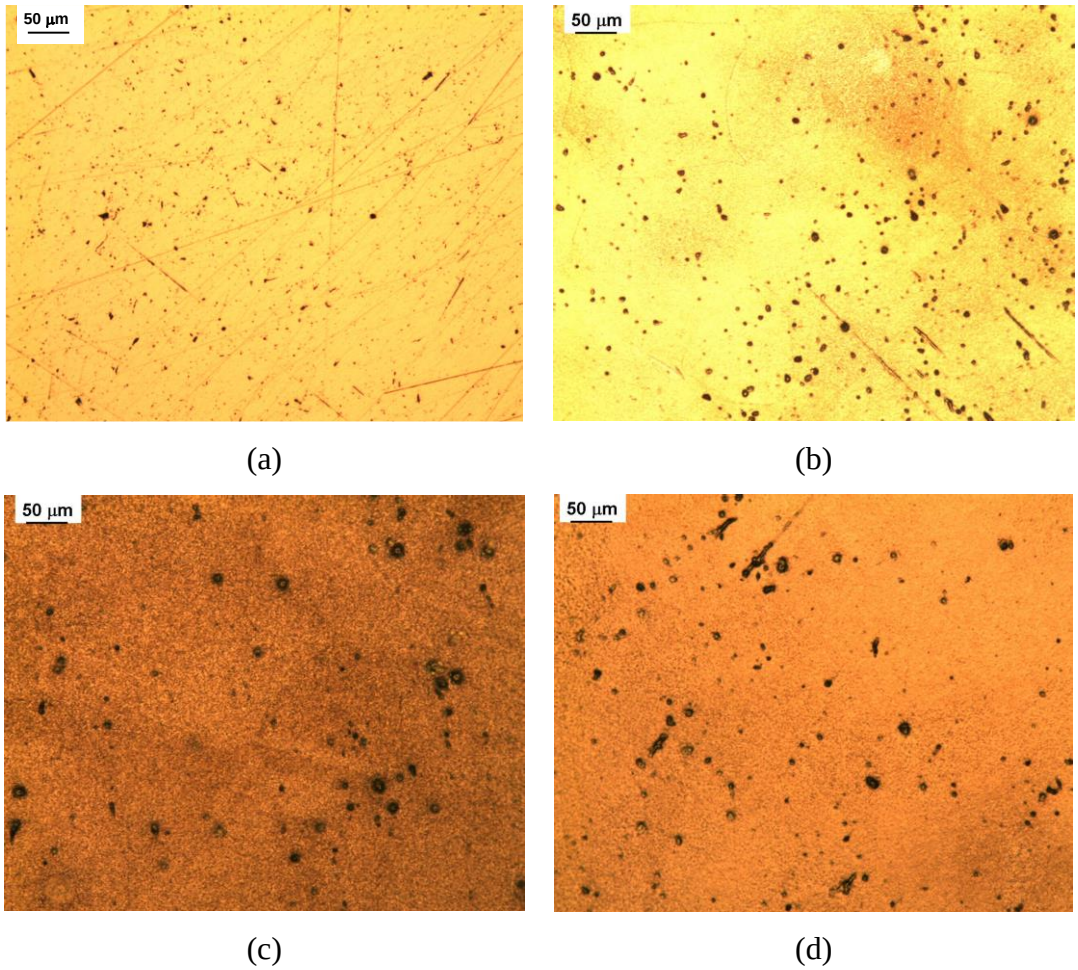

Figure 4. Images of Alloy 31 surface taken at the end of the potentiostatic tests at **(a)** 20, **(b)** 40, **(c)** 60 and **(d)** 80 ºC (100X).

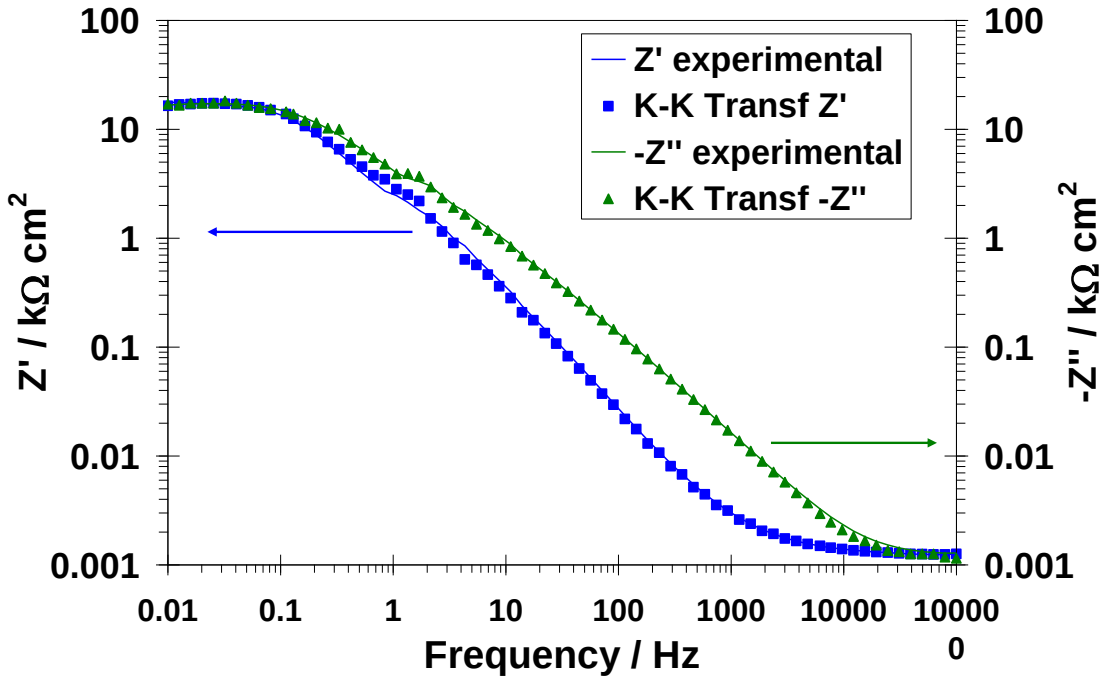

Figure 5. Kramers-Kronig transformation of the impedance diagram obtained after 1 h of stabilisation at 0.8 V vs. Ag/AgCl and 20 ºC in the contaminated phosphoric acid solution.

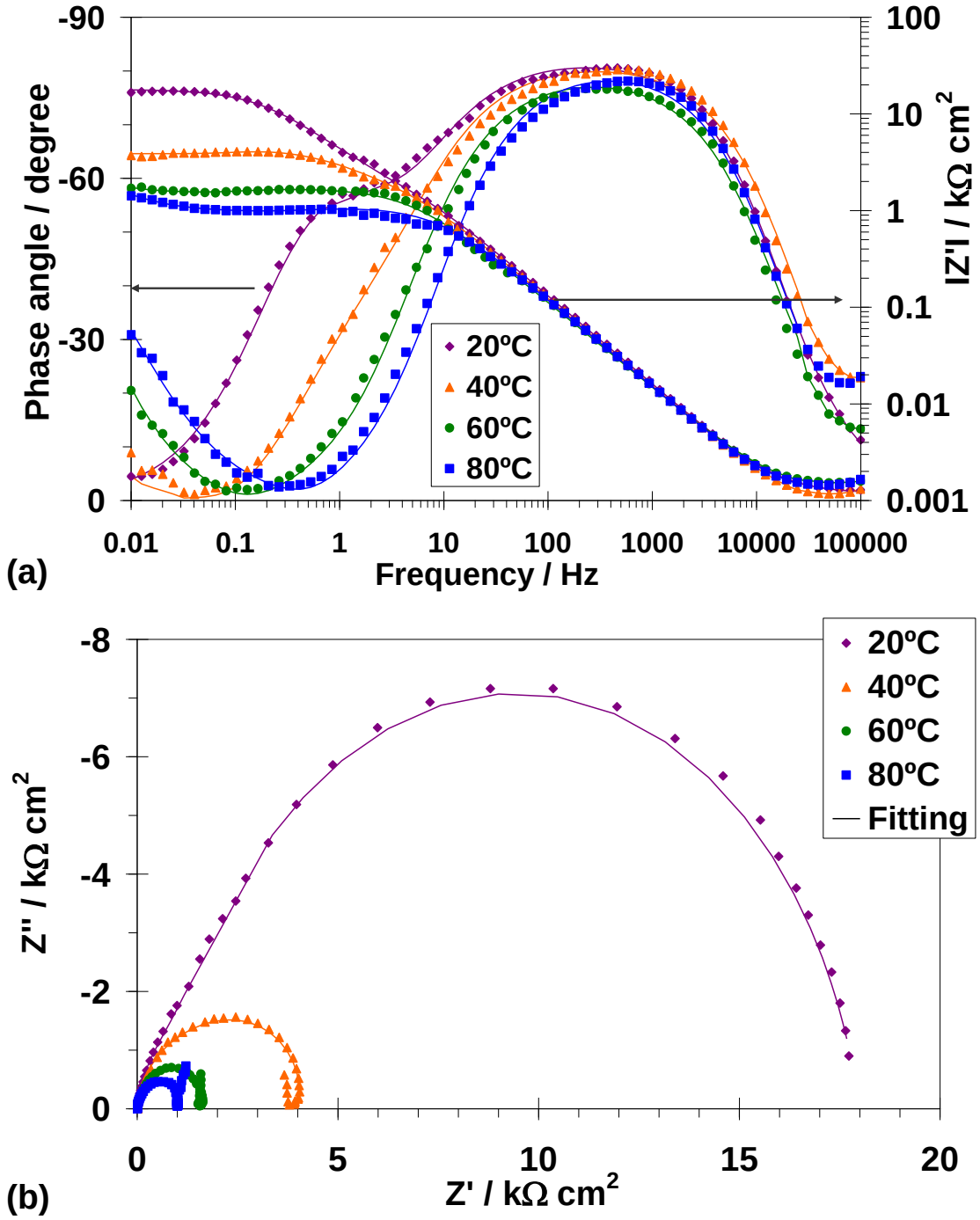

Figure 6. Nyquist diagrams **(a)** and Bode plots **(b)** of the Alloy 31 after 1 hour of passive film formation at 0.8 $V_{Ag/AgCl}$ and different temperatures.

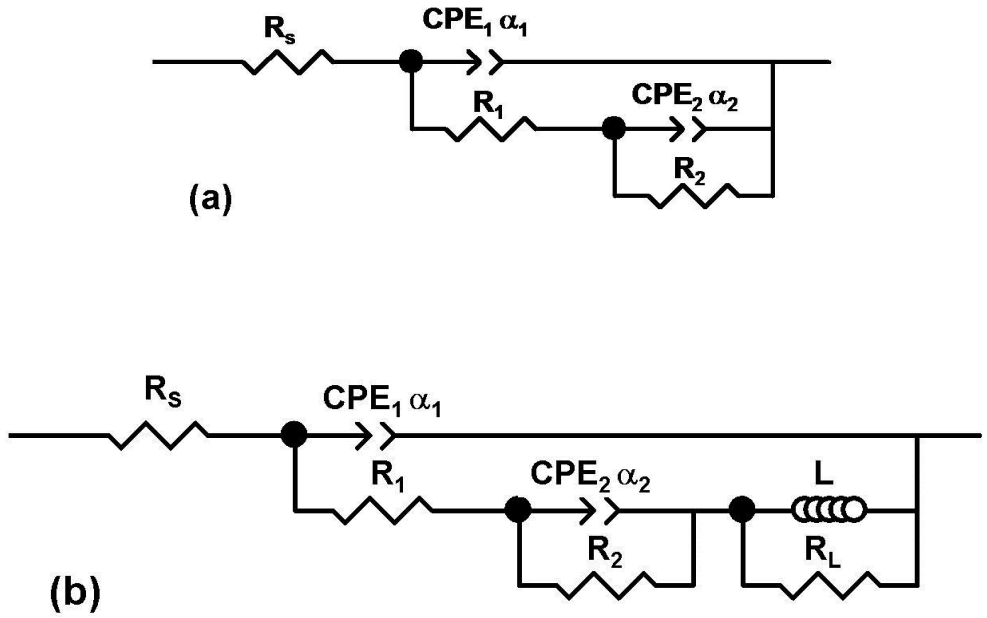

Figure 7. Equivalent electrical circuits for the analysis of the impedance spectra. R_s is the solution resistance; R_1 and CPE_1 are the resistance and CPE of the outer porous layer, respectively; R_2 and CPE_2 are the resistance and CPE of the inner oxide layer, respectively, R_L and L are the inductor elements.

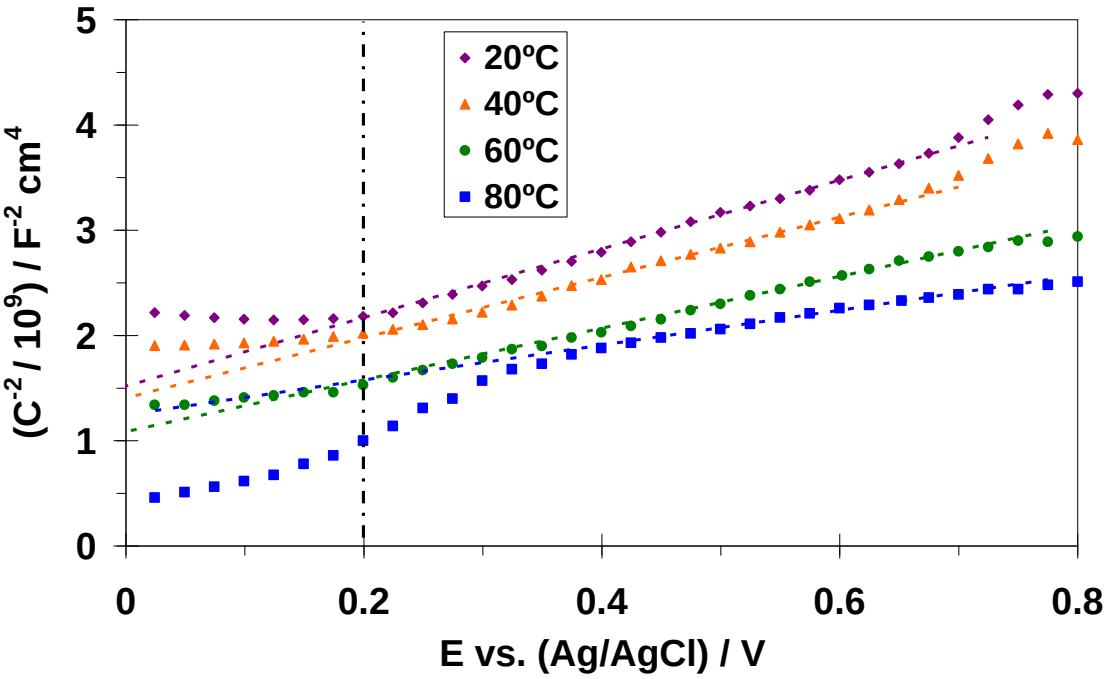

Figure 8. Mott-Schottky plot of the capacitance behaviour measured in the contaminated 40 wt.% H_3PO_4 solution at different temperatures after the electrode was passivated for 1 h at 0.8 V vs. Ag/AgCl.

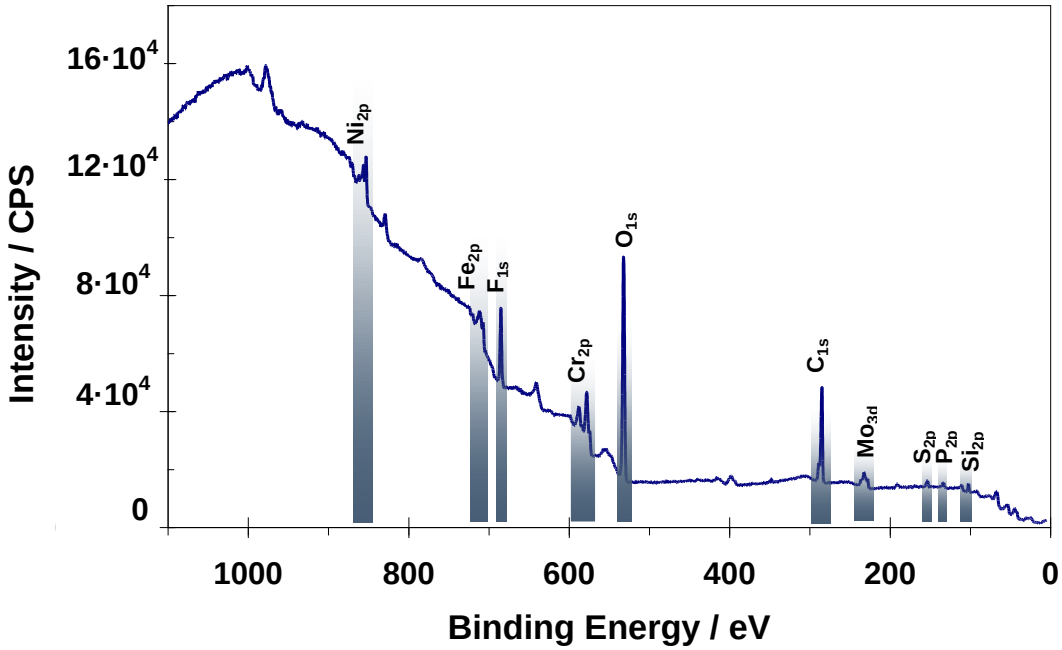

Figure 9. XPS wide scan spectrum of passive film on Alloy 31 formed at 0.8 $V_{Ag/AgCl}$ and 80 ºC in the tested solution.

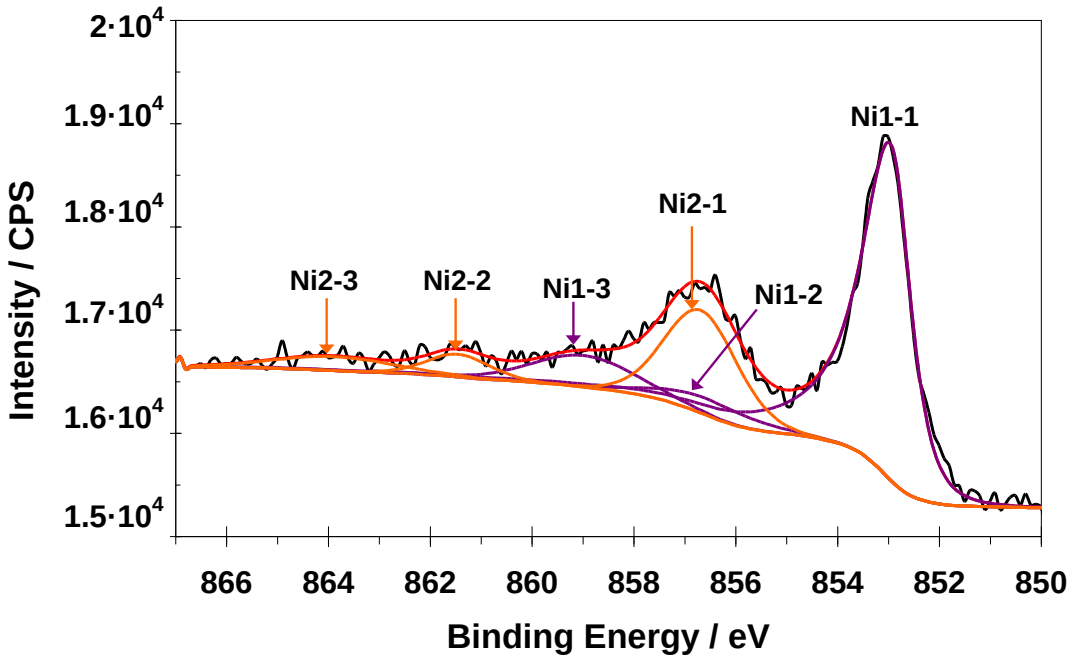

Figure 10. XPS spectra of Ni 2p of the passive films formed on Alloy 31 after passivation at 0.8 $V_{Ag/AgCl}$ and 80 ºC.

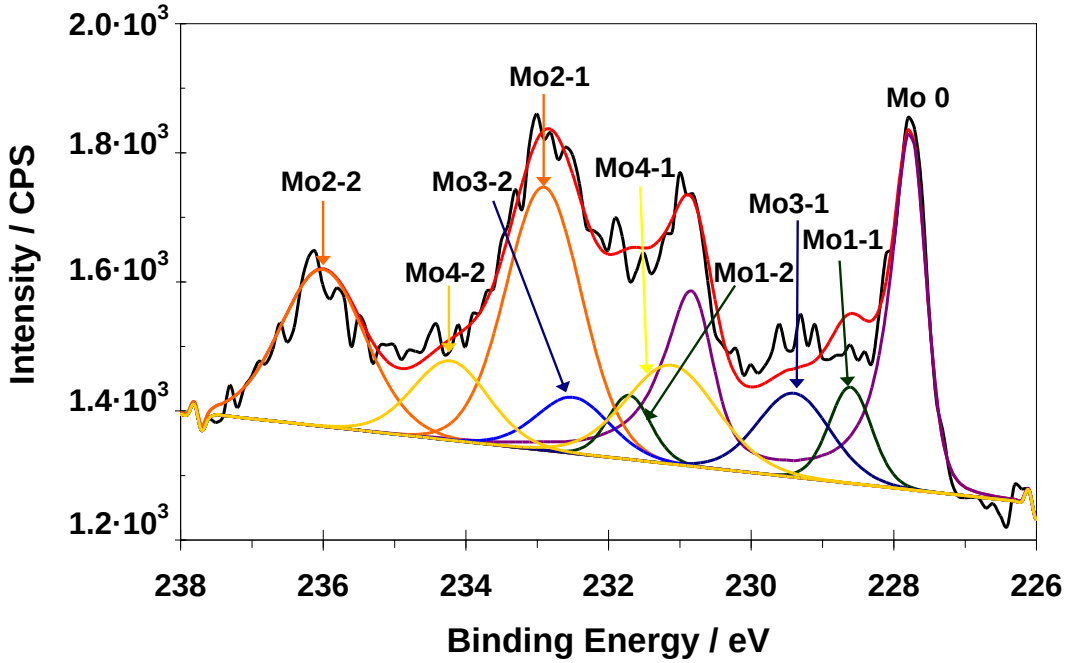

Figure 11. XPS spectra of Mo 3d of the passive films formed on Alloy 31 after passivation at 0.8 $V_{Ag/AgCl}$ and 80 ºC.

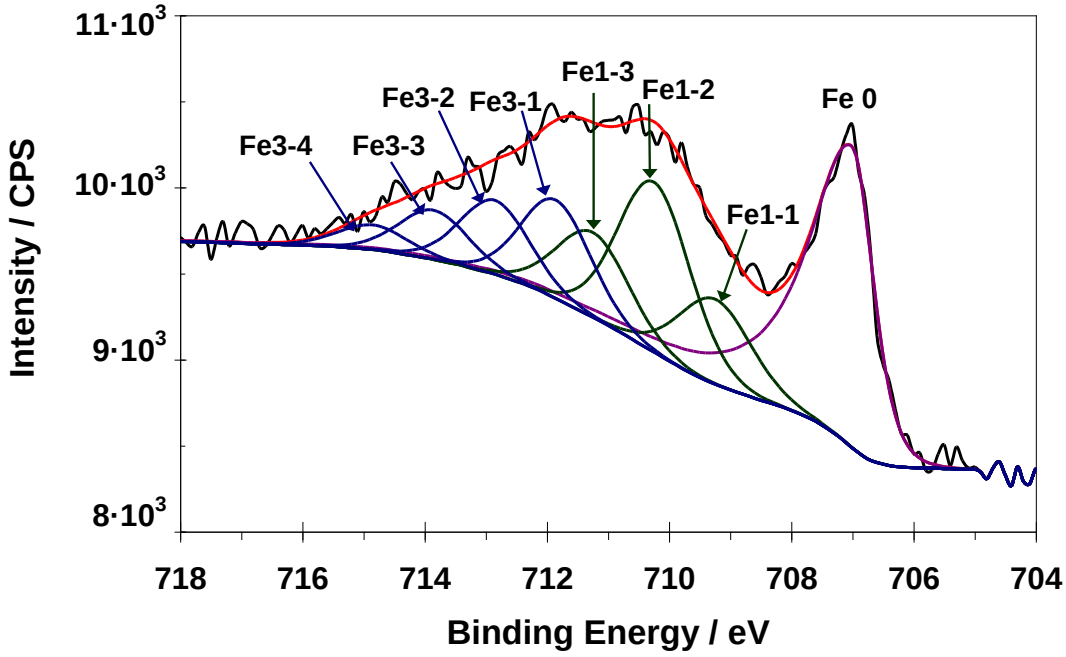

Figure 12. XPS spectra of Fe 2p of the passive films formed on Alloy 31 after passivation at 0.8 $V_{Ag/AgCl}$ and 80 ºC.

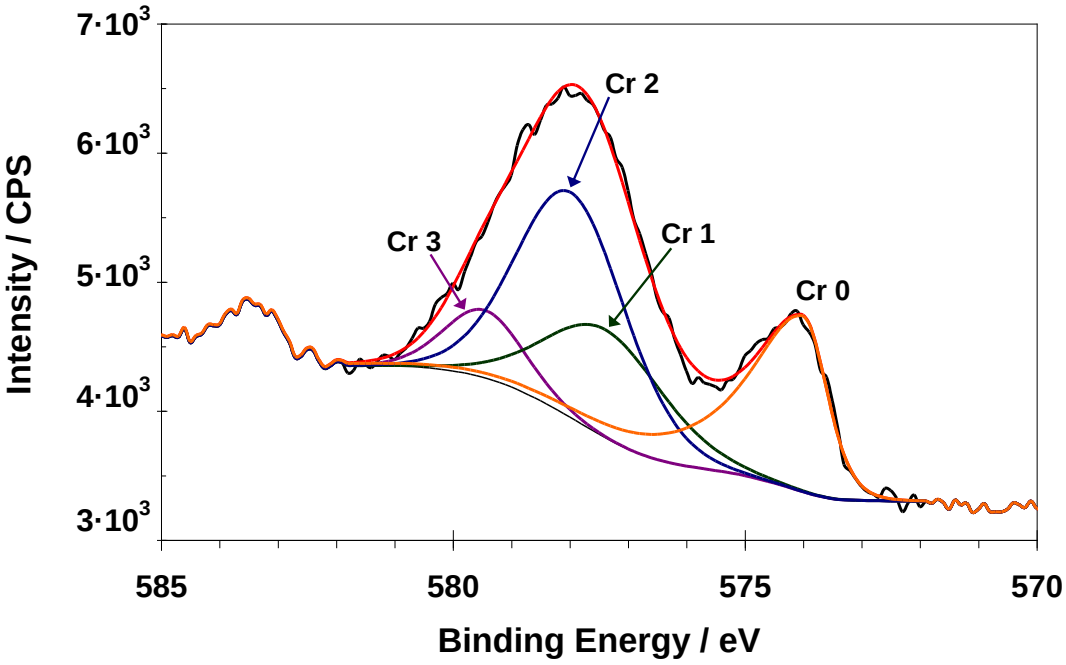

Figure 13. XPS spectra of Cr 2p of the passive films formed on Alloy 31 after passivation at 0.8 $V_{Ag/AgCl}$ and 80 ºC.